Redox Biology 67 (2023) 102887

Contents lists available at ScienceDirect

Redox Biology

journal homepage: www.elsevier.com/locate/redox

CypD induced ROS output promotes intracranial aneurysm formation and rupture by 8-OHdG/NLRP3/MMP9 pathway

Haiyan Fan [a,**,1], Hao Tian [a,1], Fa Jin [a], Xin Zhang [a], Shixing Su [a], Yanchao Liu [a], Zhuohua Wen [a], Xuying He [a], Xifeng Li [a,***], Chuanzhi Duan [a,b,*]

[a] Department of Cerebrovascular Surgery, Neurosurgery Center, Engineering Technology Research Center of Education Ministry of China on Diagnosis and Treatment of Cerebrovascular Disease, Zhujiang Hospital, Southern Medical University, Guangzhou, 510280, Guangdong, China
[b] Guangdong Provincial Key Laboratory on Brain Function Repair and Regeneration, Guangzhou, 510280, Guangdong, China

ARTICLE INFO

Keywords:
Cyclophilin D
Reactive oxygen species
Vascular smooth muscle cell
Intracranial aneurysm

ABSTRACT

Reactive Oxygen Species (ROS) are widely accepted as a pernicious factor in the progression of intracranial aneurysm (IA), which is eminently related to cell apoptosis and extracellular matrix degradation, but the mechanism remains to be elucidated. Recent evidence has identified that enhancement of Cyclophilin D (CypD) under stress conditions plays a critical role in ROS output, thus accelerating vascular destruction. However, no study has confirmed whether cypD is a detrimental mediator of cell apoptosis and extracellular matrix degradation in the setting of IA development. Our data indicated that endogenous cypD mRNA was significantly upregulated in human IA lesions and mouse IA wall, accompanied by higher level of ROS, MMPs and cell apoptosis. CypD$^{-/-}$ remarkably reversed vascular smooth muscle cells (VSMCs) apoptosis and elastic fiber degradation, and significantly decreased the incidence of aneurysm and ruptured aneurysm, together with the downregulation of ROS, 8-OHdG, NLRP3 and MMP9 in vivo and vitro. Furthermore, we demonstrated that blockade of cypD with CsA inhibited the above processes, thus preventing IA formation and rupture, these effects were highly dependent on ROS output. Mechanistically, we found that cypD directly interacts with ATP5B to promote ROS release in VSMCs, and 8-OHdG directly bind to NLRP3, which interacted with MMP9 to increased MMP9 level and activity in vivo and vitro. Our data expound an unexpected role of cypD in IA pathogenesis and an undescribed 8-OHdG/NLRP3/MMP9 pathway involved in accelerating VSMCs apoptosis and elastic fiber degradation. Repressing ROS output by CypD inhibition may be a promising therapeutic strategy for prevention IA development.

1. Introduction

Intracranial aneurysm (IA), characterized by permanent localized protuberance of the cerebral artery, is an awfully common cerebrovascular disorder that carry a high risk of morbidity with 3% in worldwide [1,2]. Rupture of IA can lead to catastrophic consequences with 50% mortality, because of extensive subarachnoid hemorrhage [3]. Until now, no effective pharmaceutical has been identified for the therapy of IA and the only options capable of restraining IA progression are endovascular treatment or craniotomy clipping [4]. The major pathological features of human IA include are progressive vascular smooth muscle cell (VSMC) death and extracellular matrix (ECM) disruption that leading to the formation and rupture of IA [5]. Therefore, unveiling the molecules mechanisms responsible for VSMC damage and ECM degradation is essential toward developing drugs to prevent IA progression.

Reactive Oxygen species (ROS), mainly produced by damaged mitochondria on the artery wall, orchestrates pathological signaling events by activating inflammation and apoptosis and triggers compromised vascular homeostasis that promote the occurrence of vascular disease such as IA [6], aortic aneurysm and atherosclerosis [7]. A recent single-cell RNA sequencing study about IA in mouse demonstrated that

* Corresponding author. Guangdong Provincial Key Laboratory on Brain Function Repair and Regeneration, Guangzhou, 510280, Guangdong, China.
** Corresponding author.
*** Corresponding author.
E-mail addresses: fan_haiyan2021@163.com (H. Fan), nflxf@126.com (X. Li), doctor_duanzj@163.com (C. Duan).
[1] HY. F and H. T are contributed equally.

https://doi.org/10.1016/j.redox.2023.102887
Received 24 August 2023; Received in revised form 11 September 2023; Accepted 11 September 2023
Available online 12 September 2023

extensive mitochondrial dysfunction occurs in VSMC of IA wall, which is intimately connected to elastin degradation and the activation of apoptotic pathways [8]. However, the regulatory mechanisms of ROS in IA development remain poorly understood.

Mitochondrial permeability transition pore (mPTP), a "transient channel" on the mitochondrial membrane, is responsible for the molecules transportation in the cytoplasm and mitochondria [9]. Prolonged mPTP opening causes ROS output, which has been implicated in a variety of diseases including neurodegenerative disorders [10], brain injury [11], and diabetes [12]. Cyclophilin D (CypD), located in the mitochondrial matrix, is a well-established regulator that opens mPTP by binding to ATP5B in the mitochondrial member, thus promoting ROS release [13]. Inhibition or knockout of cypD was extensively investigated in various disease models and an antioxidant damage and anti-inflammatory role of cypD-absence has been demonstrated in several cells such as vessels, neurons, and hepatocytes [14–16]. Moreover, cypD knockout (KO) mice employed in the angiotensin 2 induced aorta injury prevents overproduction of ROS and improves vascular relaxation, grossly similar to vascular pathological of IA, raising the possibility that cypD might also accelerate IA development [17,18]. However, the role of cypD in IA and VSMC has never been evaluated.

Given cypD critical role in ROS and vascular injury, we hypothesized that cypD activation in the cerebral artery wall induces the occurrence and rupture of IA. Here, we provide evidence showing the presence of cypD gene in IA lesions both human and mice, and uncovered a detrimental role of cypD in IA using cypD KO mice. Importantly, we shed light on the molecular mechanisms by which cypD controls VSMC apoptosis and elastic degradation. In addition, we found that the pharmacologic inhibition of cypD activation can reduce IA development in mice. Our findings demonstrate the potential for use of cypD inhibitor to treat IA.

2. Methods

2.1. Profiling of biological processes of up-regulated differentially expressed genes in human intracranial aneurysm

Bioinformatics analyses were performed using R (version 4.3.1). Microarray data (GSE75436) of 15 intracranial aneurysms and their matched superficial temporal arteries were downloaded from Gene Expression Omnibus (GEO) database (https://www.ncbi.nlm.nih.gov/geo/). Differentially expressed genes (DEGs) were identified by R package "limma" with a cutoff threshold of false discovery rate (FDR) $<$ 0.05 and $|\log2$ Fold Change (FC)$| \geqslant 1$. Expressions of specific DEGs were visualized by heatmaps and volcano map using "pheatmap" and "ggplot2" package. Potential biological processes (BP)of up-regulated DEGs were identified by Gene Ontology (GO) analysis using R package "clusterProfiler" [19].

2.2. Mouse model of intracranial aneurysm

This study was conducted in accordance with the guideline for the care and use of laboratory animals published by the US national institutes of health. All experimental protocols were approved by the Ethics Committee of Zhujiang Hospital of Southern Medical University. Male wild type and cypD knockout (KO) C57BL/6 mice (Cyagen Biosciences Inc. America), feed in the Animal Experiment Center of zhujiang Hospital of Southern Medical University, were employed to induce IA model according to the methods of previous study [20]. Simply, the right kidney was first removed from the mice. Seven days after right nephrectomy, mice were injected with elastase (35 mU) in the right basal cistern (right basal cistern positioning: the fontanel is the origin of coordinates, 1.5 mm to the right, 2.6 mm caudal, 5.1 mm ventral to the meninx surface) and deoxycorticosterone acetate (DOCA) sustained-release tablets (21 days, 50 mg) were implanted subcutaneously on the same day. Then start drinking with 0.9% saline for 21days.

Systolic blood pressure was measured every 7days using Non-invasive Blood Pressure Meter (BP-2010 series, Softron, Japan). The mice were checked daily for neurological symptoms as previously mentioned. Positive neurological symptoms including: more than 10% weight loss within 24 h; circling to one side; paresis; no spontaneous activity. Once the mice showed positive neurological symptoms, they were immediately anesthetized for further experiments.

2.3. Primary mouse cerebral artery vascular smooth muscle cells

The cerebral artery of adult mice was isolated under microscope, the outer membrane of the blood vessel was removed, and the inner layer was gently scraped out. Cut the medium layer, add 0.1% collagenase for digestion in a 30° water bath for 5 h, then add 0.25% pancreatin for further digestion for 15min. After standing for 10min, the supernatant was collected and filtered through 100 mesh and 200 mesh screens. Cell suspension was centrifuged at 1000r for 5min, and the cells were re-suspended with complete medium, then moved to T25 bottle for culture. Half an hour later, the supernatant was taken to a new bottle for further culture, and the primary smooth muscle cells were obtained.

2.4. Drug administration

Cyclosporine A (CsA, HY-B0579, MedChemExpress), cypD inhibitor, was prepared as previously established [21]. Briefly, CsA was first dissolved in DMSO at 50 mg/ml and diluted with saline before to use. The doses of 10 mg/kg/daily were intraperitoneally injected after IA model induction.

2.5. Immunofluorescence

Immunofluorescence (IF) staining was conducted as formerly described [22]. Paraffin-embedded brain sections (4-μm thickness) were prepared as above-mentioned and antigen retrieval was performed with EDTA antigen retrieval solution (C1034, Solarbio, China) in a microwave oven lasting for 25 min. Subsequently, the sections were blocked with 5% goat serum (SL038, Solarbio, china) at room temperature for 30 min and then incubated overnight at 4 °C with the primary antibody as follows: anti-alpha smooth muscle Actin antibody (1:1000, ab124964, abcam), Anti-8-OHdG antibody (1:500, ab62623, abcam), Anti-NLRP3 antibody (1:50, NBP2-12446, Novus), Anti-MMP9 antibody (1:300, GB11132, Servicebio), Anti -alpha smooth muscle Actin antibody (1:500, GB13044, Servicebio). Adjacently, the slices were washed with PBS and then incubated with corresponding secondary antibodies for 1 h at 37 °C. secondary antibodies as follows: Alexa Fluor 488 goat anti-rabbit IgG (1:400, Abcam, ab150077); Alexa Fluor 594 goat anti-rabbit IgG (1:400, Abcam, ab150080); Alexa Fluor 594 goat anti-mouse IgG (1:400, abcam, ab150116); Alexa Fluor 488 goat anti-mouse IgG (1:400, abcam, ab150113); Alexa Fluor 647 goat anti-mouse IgG (1:400, abcam, ab150115). After washed with PBS, DAPI was employed to dye the nucleus for 15 min. Images were captured by a fluorescence microscope.

2.6. Immunohistochemistry

Immunohistochemical (IHC) staining was performed based on the commercial kit (PV-9001, ZSGB-Bio, China). After antigen repair, the endogenous peroxidase blocker was incubated at room temperature for 10 min and then slices were incubated overnight at 4 °C with *Anti*-Cyclophilin F antibody (1:500, ab231155, abcam). Adjacently, sections were incubated with biotinylated goat anti-mouse IgG secondary antibody for 20 min at 37 °C and later with HRP-streptavidin reagent. Ultimately, immunoreactivity was visualized using 3,3-diaminobenzidine (DAB, Boster), followed by restaining with hematoxylin. Images were obtained via a light microscope (Leica, DM2500, Germany).

2.7. Hematoxylin-eosin staining and elastic fiber staining

Paraffin-embedded brain sections (4-μm thickness) were prepared as above-mentioned. After dewaxing, the sections were stained with H&E solution (C0105S, Beyotime, China) and victoria blue solution (G1596, Solarbio, China) according to commercial kits, respectively. Images were obtained via a light microscope (Leica, DM2500, Germany).

2.8. Terminal deoxynucleotidyl transferase (TdT)-mediated dUTP nick end labeling staining

Smooth muscle cell apoptosis was detected with a TUNEL kit (C1089, Beyotime, China) in strict accordance with the instructions. After dewaxing and hydration, sections were incubated with proteinase K for 20min at room temperature. After washed with PBS three times, sections were stained with TUNEL reaction mixture for 1 h at 37 °C.Adjacently, slices were incubated overnight at 4 °C with rabbit anti-alpha smooth muscle actin antibody (1:1000, ab124964, abcam). After washed with PBS three times, sections were stained with anti-rabbit 488 and DAPI for 1 h and 20min at room temperature. Finally the slices were sealed and photographed under the microscope for observation.

2.9. Transmission electron microscopy and scanning electron microscopy

Transmission electron microscopy (TEM) was performed as previously described [22]. Compendiously, the cerebral vessels with brain tissue was promptly isolated and quickly put into 2.5% glutaraldehyde (M8K7018, nacalai tesque, Japan) in alive mice. After fixation, dehydration, infiltration and embedding, the 60–80 nm ultrathin tissue slices were obtained by ultra-micro microscopies (Leica UC7, Leica), and then the structure of cerebral vessels was observed by HITACHI HT7700 transmission electron microscopy.

Scanning electron microscopy is similar to TEM mentioned above. Compendiously, the cerebral vessels with brain tissue was promptly isolated and quickly put into 2.5% glutaraldehyde (M8K7018, nacalai tesque, Japan) in alive mice. After dehydration, drying, conductive treatment, and then the structure of cerebral vessels was observed by ZEISS gemini300.

2.10. In situ zymography

In situ zymography staining was performed according to the kit instructions (GMS80062.1, GENMED, China). First, the 10um fast frozen sections were prepared, the GENMED solution was added to stand for 10min at 4°, then incubated at 37° for 60 min, and finally photographed at 488 nm for observation.

2.11. Fluorescence in situ hybridization

CypD mRNA probe was designed and synthesized by company (GenePharma, China). After frozen section preparation, citrate buffer was incubated at room temperature for 15min, protease K was digested at 37 °C for 30min, 2xSSC was washed three times, and then dehydrated in 70%–80%-90%–100% gradient alcohol successively, denatured

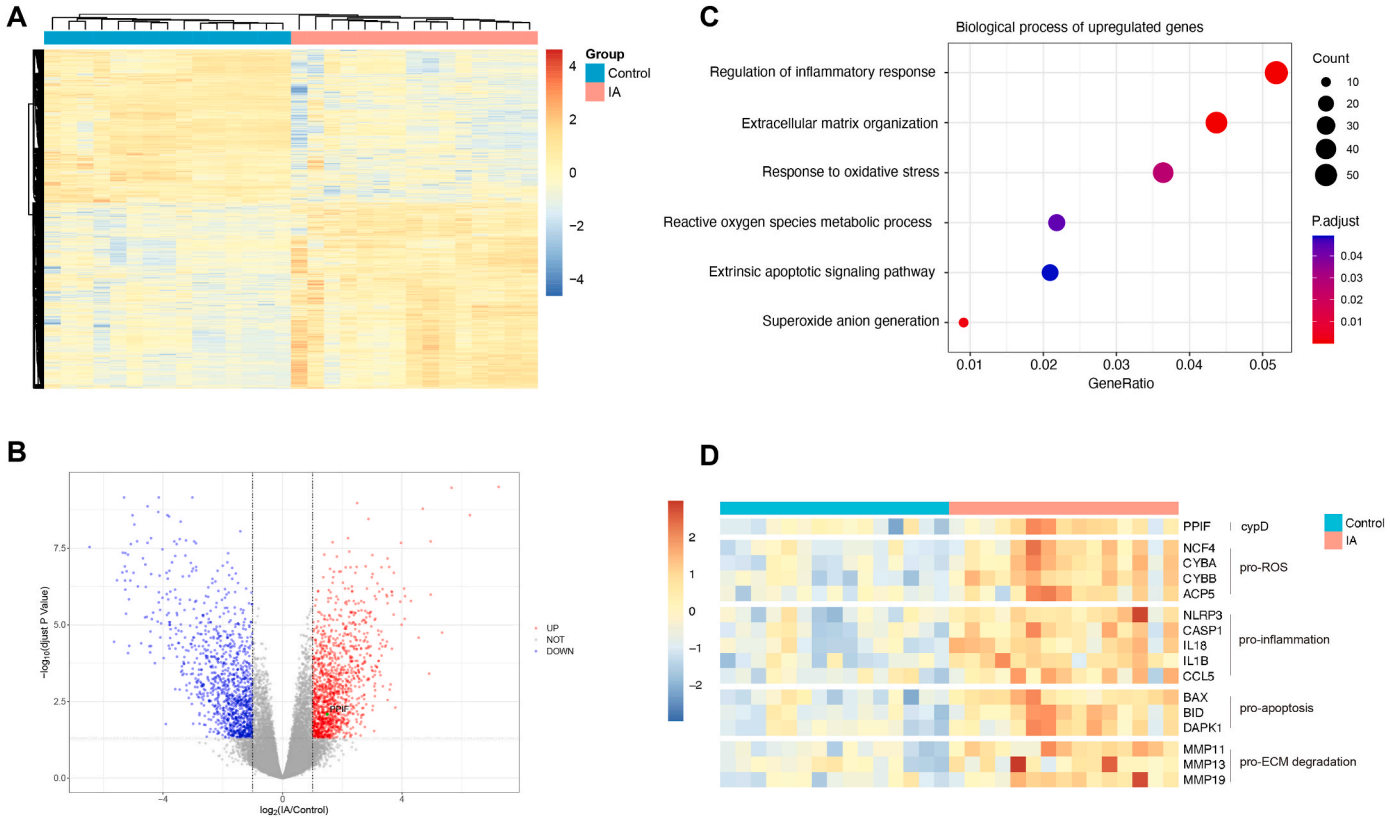

Fig. 1. Presence of cypD mRNA in human intracranial aneurysm tissues
A, Heatmap showing the transcript expression levels of 2337 differentially expressed genes (DEGs) in GSE75436 of 15 intracranial aneurysm tissues of human and their matched normal superficial temporal arteries. B, Volcano plot simultaneously demonstrating the fold changes (UIA/control) and Wilcoxon test results of 2337 DEGs. Red dots show the 1254 genes that were signifcantly upregulated. Blue dots show the 1083 genes that signifcantly downregulated. Specifc genes of interest are labeled with green dots. Abbreviations: ppif stands for cypD. C, Gene ontology (GO) analysis of upregulated DEGs in human IA tissues showing the diversified highly expressed biologic processes involved in oxidative stress, inflammation, apoptosis and ECM organization. D, Heat map showing that the differential expressions of specific upregulated DEGs related to cypD, ROS, inflammation, apoptosis and ECM degradation between IA tissues and their matched normal superficial temporal arteries. n = 15 vs n = 15.

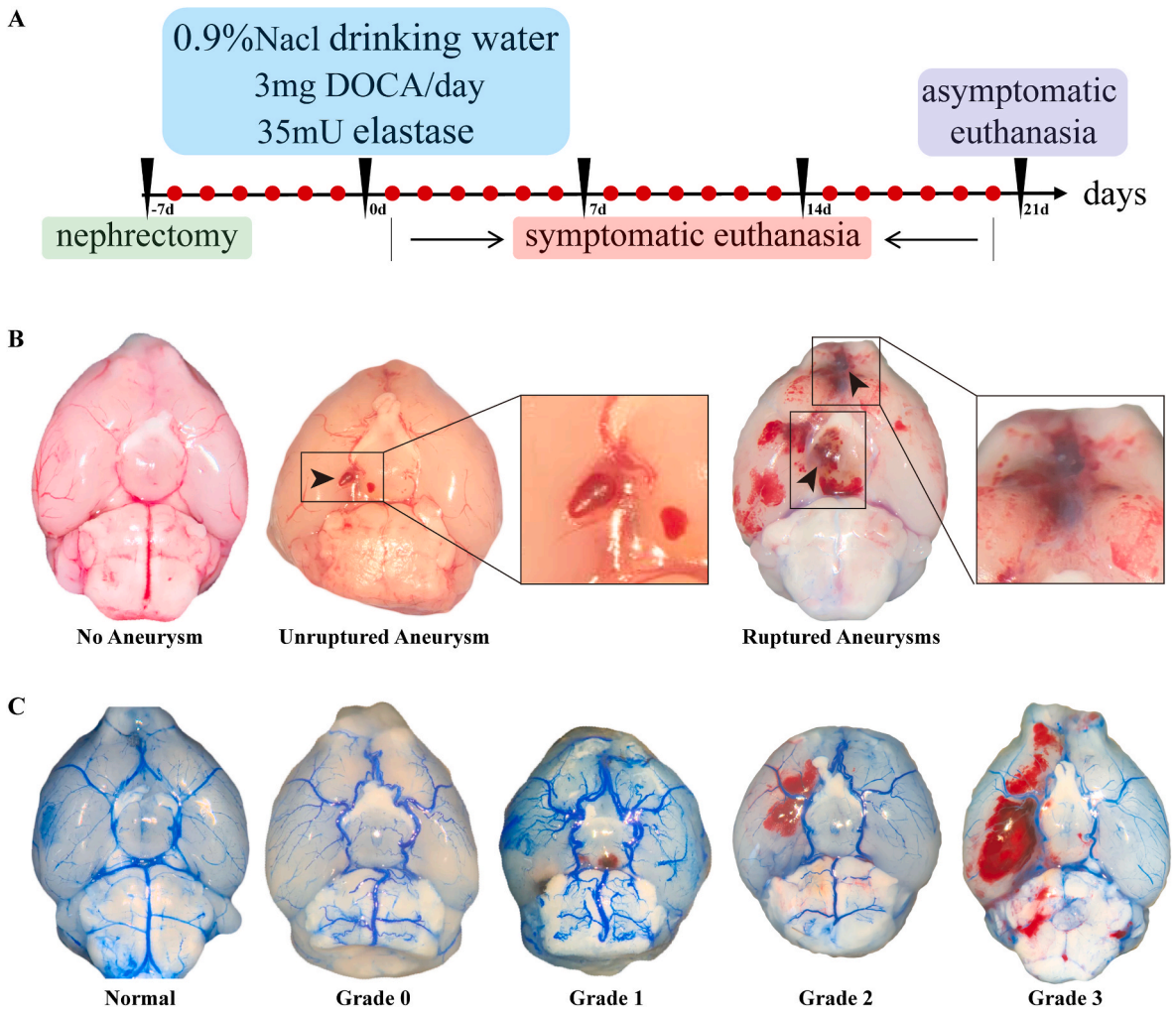

Fig. 2. Typical images of intracranial aneurysm (IA) model
A, Schematic diagram of intracranial aneurysm mouse molding method. B, Representative photographs of cerebral vascular in the bottom of mice brains. Left panel showing the normal cerebral vessels; middle panel shows the intracranial aneurysm (IA) of mice, the black arrow indicates unruptured aneurysm; right panel shows the ruptured IA of mice, the white arrow indicates ruptured aneurysm. C, Typical images of bleeding grades in ruptured aneurysms.

solution was incubated for 8min at room temperature, then dehydrated again, probe hybridization was performed for 14 h at 37 °C, and samples were washed twice with 2xSSC for 10min each time. Then DAPI was incubated at room temperature for 10min, the tablets were sealed and observed under confocal microscope.

2.12. Dihydroethidium staining

Dihydroethidium (DHE) staining was performed according to the kit instructions (BB-470516, Bestbio, China). First, the 10um fast frozen sections were prepared, the cleaning solution was added to stand for 5min, and then the DHE probe working solution was added, incubated at 37°for 30min, washed with PBS for 3 times, and finally the slices were sealed and photographed under the microscope for observation.

2.13. Immunoprecipitation

The experiment was performed according to the instructions of the co-immunoprecipitation (co-IP) kit (88804, Thermo Scientific). Simply, the cell lysates were incubated with IP antibodies (NLRP3, ab270449, abcam) overnight at 4 °C, and the antigen-antibody complex was bound to the protein A/G magnetic beads at room temperature for 1 h. The magnetic beads are washed twice with the IP cracking/washing buffer and once with pure water, followed by the elution of the magnetic beads to obtain the antigen/antibody complex for subsequent experiments.

2.14. Reactive Oxygen Species staining

Reactive Oxygen Species (ROS) staining was performed according to the kit instructions (S0033, Beyotime, China). First, the DCFH-DA probe solution was added, incubated at 37 °C for 20min, then washed with serum-free cell medium for 3 times, and finally photographed under a microscope.

2.15. Dot blot and western blot

After protein extraction, the sample was divided into two parts. One part was not added with reducing agent, and dot blot was performed. The steps were as follows: the sample was directly added on the membrane, irradiated under ultraviolet light for 10min, closed by 5% BSA for 2 h, the primary antibody was incubated at 4° overnight, the secondary antibody was incubated at room temperature for 1 h, and finally ECL luminous development was performed. The other part was added with a reducing agent, and Western blot was performed according to our previous steps. The sample was added to the preform gel, followed by 150v electrophoresis for 1 h, 200 mA membrane transfer for 2 h, electrophoresis at 150v for 1 h, film transfer at 200 mA for 2 h. The subsequent steps were consistent with dot blot, followed by closure, primary

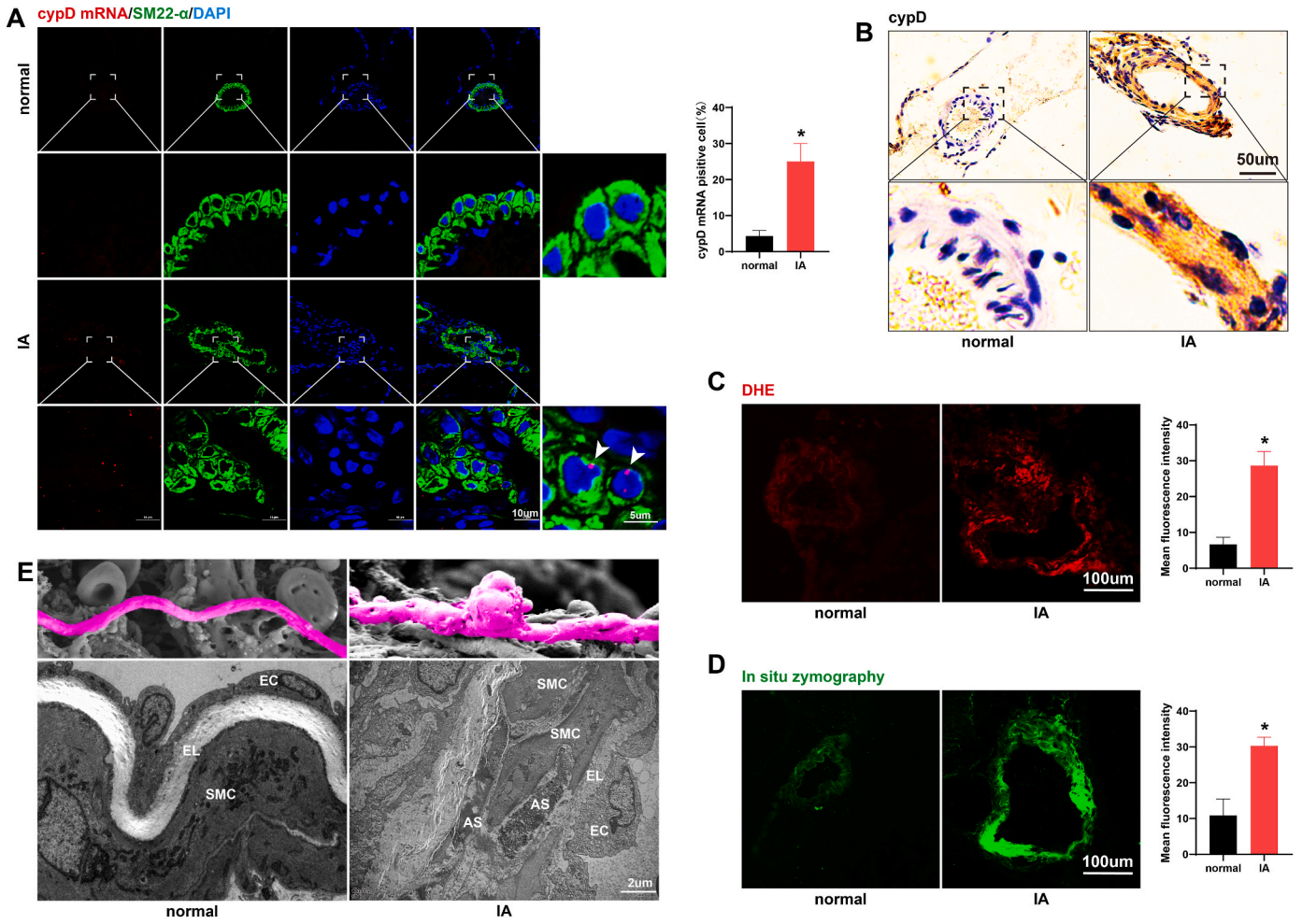

Fig. 3. Presence of cypD in intracranial aneurysm tissues from mouse
A, Representative microphotographs of FISH staining for cypD mRNA (red) co-localization on VSMCs (SM22-α, green) in normal cerebral vessels and IA lesion. B, Representative images of immunohistochemical staining for cypD in normal cerebral vessels and IA lesion. C-D, Representative images of DHE staining (red) and in situ zymography staining (green) in normal cerebral vessels and IA lesion. E, Representative pictures of scanning electron microscope (SEM) and transmission electron microscope (TEM) in normal cerebral vessels and IA lesion. Upper panel shows the morphology of normal vessel and IA; lower panel shows the vascular wall structure of normal cerebral vessels and IA. SMC = smooth muscle cell, AS = apoptosis smooth muscle cell, EL = elastic fibre, EC = endothelial cell.

antibody and secondary antibody. Finally, ECL luminous development was performed.

2.16. Statistical analysis

All of the Data were presented as means ± standard deviation (SD) and statistical analyses were performed using SPSS 19.0 software (SPSS, IBM, USA). $P < 0.05$ were considered statistically significant. The difference of continuous variables was compared using the Wilcoxon test. Fisher exact test was used to analyze the incidences of aneurysm formation and aneurysm rupture. Comparison between groups was determined by one-way analysis of variance (ANOVA) and followed by LSD test dunnett's T3 test for the two group's comparison within the multiple groups.

3. Results

3.1. Presence of cypD mRNA in human intracranial aneurysm tissues

To identify novel molecular mechanisms underlying IA development, we downloaded and analyzed the microarray dataset GSE75436 of human superficial temporal arteries and intracranial aneurysms. As a result, a total of 2337 differentially expressed genes (DEGs), consisting of 1254 upregulated DEGs and 1083 downregulated DEGs, were obtained with a cutoff threshold of FDR<0.05 and |log2 fold change|≥1 (Fig. 1A and B). Furthermore, we focused on the profiling of biological processes of up-regulated DEGs in IA using GO analysis. Enrichment analysis showed that upregulated genes in IA tissues involved multiple biologic processes including the superoxide anion generation, ROS metabolic process, oxidative stress, inflammatory response, extracellular matrix (ECM) organization and cell apoptosis (Fig. 1C). In particular, analysis of DEGs in the IA showed the upregulation of key molecules including cypD, ROS production, inflammatory pathway, ECM degeneration and apoptosis pathway (Fig. 1D). Together, these findings support that aneurysm present elastic fiber degradation and smooth muscle cell apoptosis because of mitochondrial dysfunction and inflammatory response.

3.2. Presence of cypD in intracranial aneurysm tissues from mouse

To assess whether the same pathological feature occurs in IA wall from mouse, we next evaluated the changes of cypD mRNA, cypD protein, ROS content and MMPs activity in a well-established experimental IA models of mice. In our IA models, mice first underwent unilateral nephrectomy, followed by injection of elastase in right basal cisterns and DOCA subcutaneous implantation one week later, and a high salt

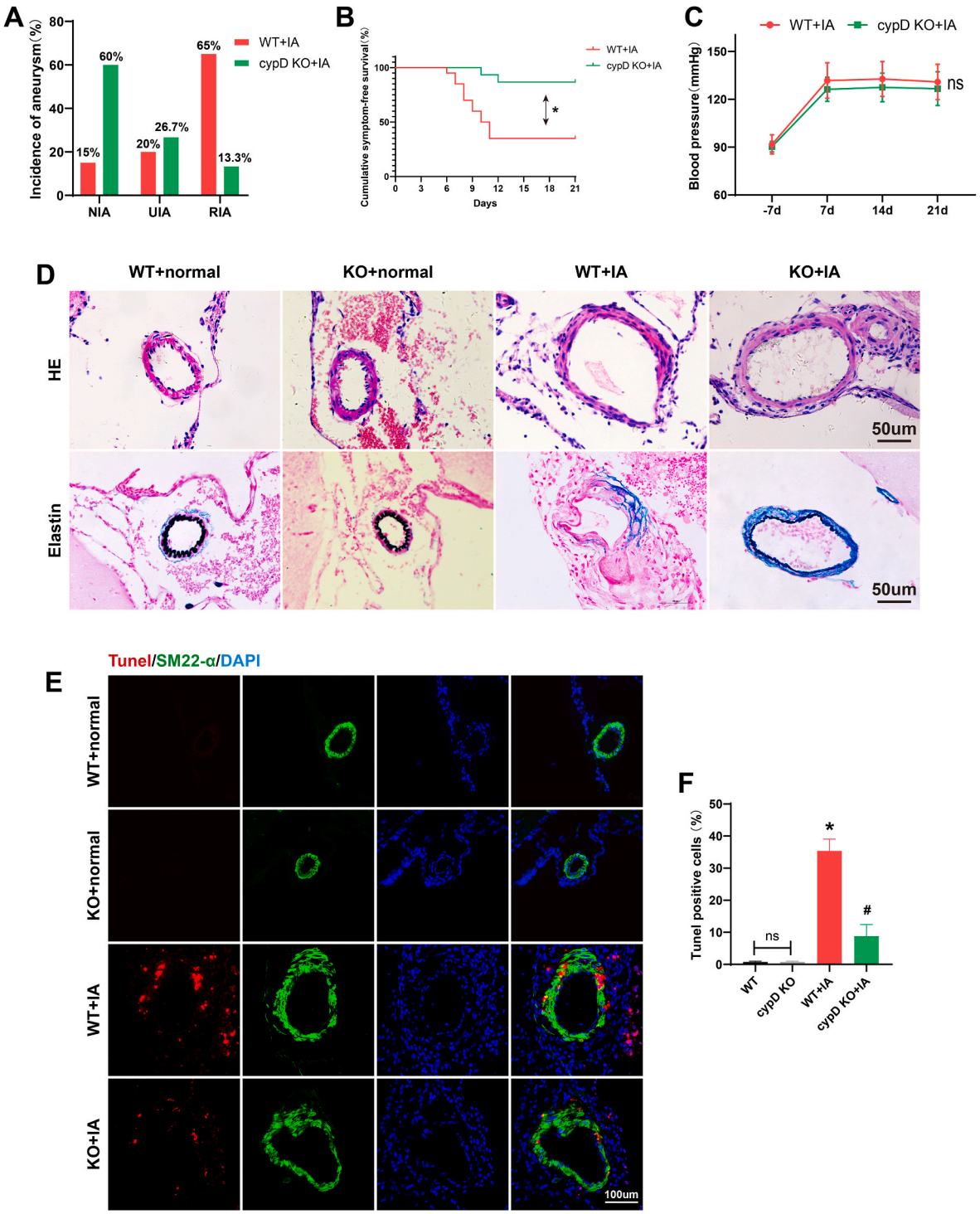

Fig. 4. Reduced the development of intracranial aneurysm (IA) in cypD KO mice
A, The incidence of IA and ruptured IA in WT mice and cypD KO mice; B, The cumulative symptom-free survival in two groups. *P < 0.05. C, Blood pressure results in both groups. D, Representative images of hematoxylin-eosin (HE) staining and elastic fiber satining in different groups. n = 4 per group. E, Representative microphotographs and quantitative analyses of TUNEL staining (red) co-localization on VSMCs (SM22-α, green) in different groups. n = 4 per group. Bars represent mean ± SD. ns stands for no significance; *P < 0.05 vs. WT group; #P < 0.05 vs. WT + IA group.

beverage for the next 3 weeks (Fig. 2A). Fig. 2B showed typical images of normal cerebral arteries, unruptured aneurysms, and ruptured aneurysms. Fig. 2C exhibited representative picture of three bleeding levels of ruptured aneurysms. Consistent with the results of transcriptome studies (Fig. 1), IA tissues in mouse showed both mRNA (Fig. 3A) and protein (Fig. 3B) of cypD levels were significantly upregulated in vascular smooth muscle cells (VSMCs) together with increased production of ROS (Fig. 3C) and enhancive MMPs activity (Fig. 3D) were also observed in the IA wall. Additionally, scanning electron microscope and transmission electron microscope analysis showed that, compared with healthy control artery, aneurysm samples showed obviously elastic fiber degradation and smooth muscle cell apoptosis (Fig. 3E). Together, these results suggest that cypD may play a role in the pathogenesis of IA, such as antioxidant and anti-inflammatory.

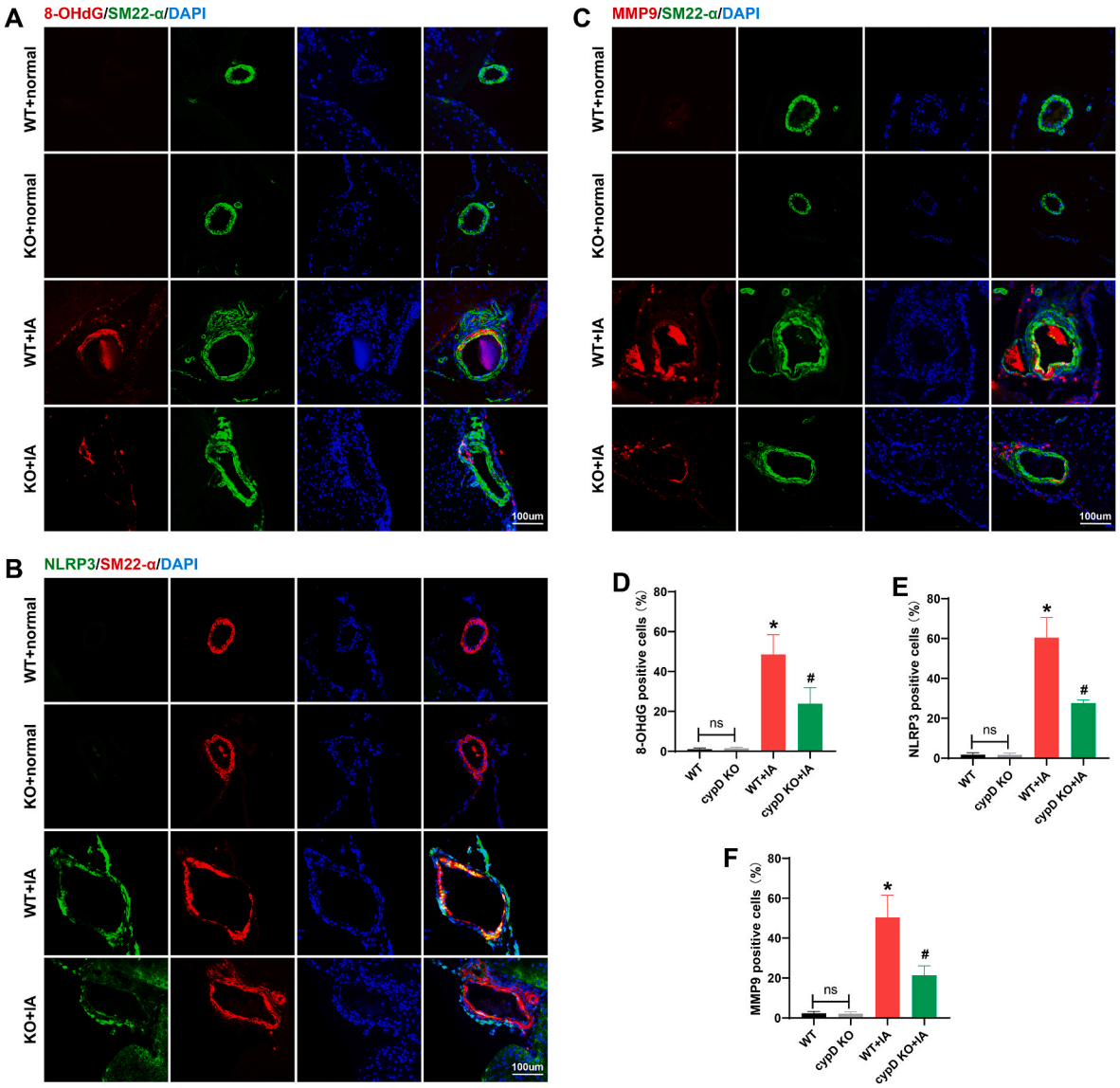

Fig. 5. Downregulation of 8-OHdG/NLRP3/MMP9 pathway in cypD KO mice with IA
A-F, Representative microphotographs of double immunofluorescence staining for 8-OHdG (red), NLRP3 (green) and MMP9 (red) in the VSMCs in diverse groups. n = 4 per group. Bars represent mean ± SD. ns stands for no significance; *P < 0.05 vs. WT group; #P < 0.05 vs. WT + IA group.

3.3. Reduced the development of intracranial aneurysm and 8-OHdG/NLRP3/MMP9 pathway in cypD KO mice

To investigate the association of cypD in the occurrence and rupture of IA, we performed a succession of experiments using wild type (WT) and cypD knockout (cypD KO) mice. In sharp contrast to WT mice, cypD KO mice challenged with IA model protocol showed a lower incidence of IA (85% vs 40%, n = 17 vs n = 12, P = 0.0029, Fig. 4A) and rupture IA (76.47% vs 33.33%, n = 13 vs n = 4, P = 0.0287, Fig. 4A). Similarly, a symptom-free curve also showed a significant reduction of ruptured aneurysm in cypD KO mice (Fig. 4B). Moreover, there was no difference in blood pressure values between the two groups (Fig. 4C).

We performed further analyses of mouse cerebral artery to determine the role of cypD in elastic fiber degradation and VSMCs apoptosis. Aneurysm wall in WT mice decreased elastic fiber fragment (Fig. 4D) and increased the number of TUNEL-positive VSMCs (Fig. 4E and F). However, these events were reversed in cypD KO mice of IA model (Fig. 4D–F). We also examined the effect of cypD on 8-OHdG, NLRP3 and MMP9, which plays a critical role in elastic fiber degradation and apoptosis. We found that 8-OHdG/NLRP3/MMP9 pathway was activated in IA wall of WT mice (Fig. 5), which was consistent with the transcriptomics data of human aneurysm tissue (Fig. 1). Conversely, knockout of cypD protected against the same pathway, indicating that cypD is involved in activating 8-OHdG/NLRP3/MMP9 pathway (Fig. 5). Together, these findings suggest that cypD contributes to IA development with accelerating VSMCs apoptosis and elastic fiber degradation partly by stimulating 8-OHdG/NLRP3/MMP9 pathway.

3.4. CypD bonds together with ATP5B to release ROS in cerebral artery VSMCs

Next, we investigated the functional role of cypD in 8-OHdG/NLRP3/MMP9 pathway in VSMCs, we performed in vitro analysis in primary vascular smooth muscle cells from WT mouse and cypD KO mouse (Fig. 6A). Immunoprecipitation data showed that cypD was directly bound to ATP5B in VSMCs treatment with H_2O_2 (Fig. 6B). Then, we stimulated VSMCs with PBS and CCCP, followed by ROS positive control experiments, and the results showed that PBS did not stimulate ROS production (Supplementary Fig. 1). Furthermore, treating VSMCs with H_2O_2 for 24 h aggrandized ROS production, which was partially

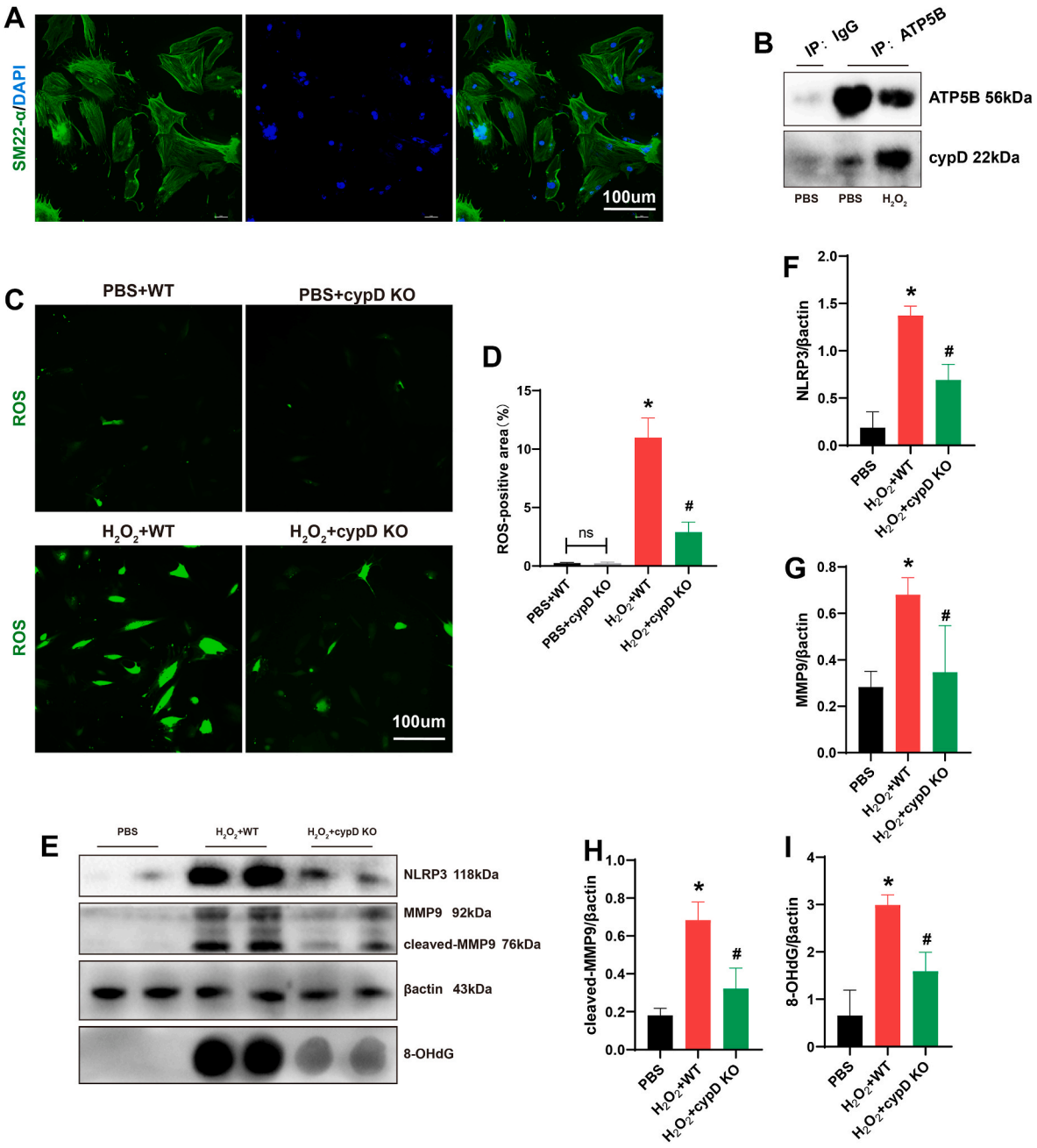

Fig. 6. CypD bonds together with ATP5B to release ROS in cerebral artery VSMCs
A, Representative picture of immunofluorescence staining for primary VSMCs (SM22-α, green). B, Cell lysates were collected and immunoprecipitated with *anti*-ATP5B Ab and *anti*-IgG Ab, then western blotted with *anti*-ATP5B Ab and *anti*-cypD Ab. C-D, Representative picture and quantitative analyses of ROS staining (green) in diverse groups. n = 4 per group. Bars represent mean ± SD. *P < 0.05 vs. PBS + WT group; #P < 0.05 vs. H_2O_2+WT group. E,I, Representative dot blot images and quantitative analyses of 8-OHdG in three groups. n = 4 per group. Bars represent mean ± SD. *P < 0.05 vs. PBS group; #P < 0.05 vs. H_2O_2+WT group. E-H, Representative Western blot images and quantitative analyses of NLRP3 and MMP9 in three groups. n = 4 per group. Bars represent mean ± SD. *P < 0.05 vs. PBS group; #P < 0.05 vs. H_2O_2+WT group.

blocked in primary VSMC from cypD KO mouse (Fig. 6C and D). We then examined the role of cypD in 8-OHdG/NLRP3/MMP9 pathway. Our results showed that treating primary VSMCs from WT mouse with H_2O_2 for 24 h increased levels of 8-OHdG, NLRP3, MMP9 and cleaved MMP9, which was also partially prevented in primary VSMC from cypD KO mouse (Fig. 6E–I). These data indicate that cypD induced ROS output by binding to ATP5B.

3.5. *NLRP3 binds to 8-OHdG and MMP9 in vascular smooth muscle cell*

Although the effects of cypD on 8-OHdG/NLRP3/MMP9 pathway have been well established, the interaction between the pathway molecules remains poorly understood. To investigated the potential association between 8-OHdG, NLRP3 and MMP9, we performed in vivo and in vitro analysis. Multiple immunofluorescence staining in vivo showed that NLRP3 colocalized with 8-OHdG and MMP9 in VSMCs of the IA lesion, indicating an association between 8-OHdG production and NLRP3-MMP9 activation in the VSMCs of IA tissues (Fig. 7A). To further ascertain the connection in regard to 8-OHdG/NLRP3/MMP9, the results of coimmunoprecipitation assay and dot blot experiments in vitro showed that NLRP3 was bound to 8-OHdG and MMP9 in VSMCs treatment with H_2O_2 for 24 h (Fig. 7B and C). Overall, these findings suggest

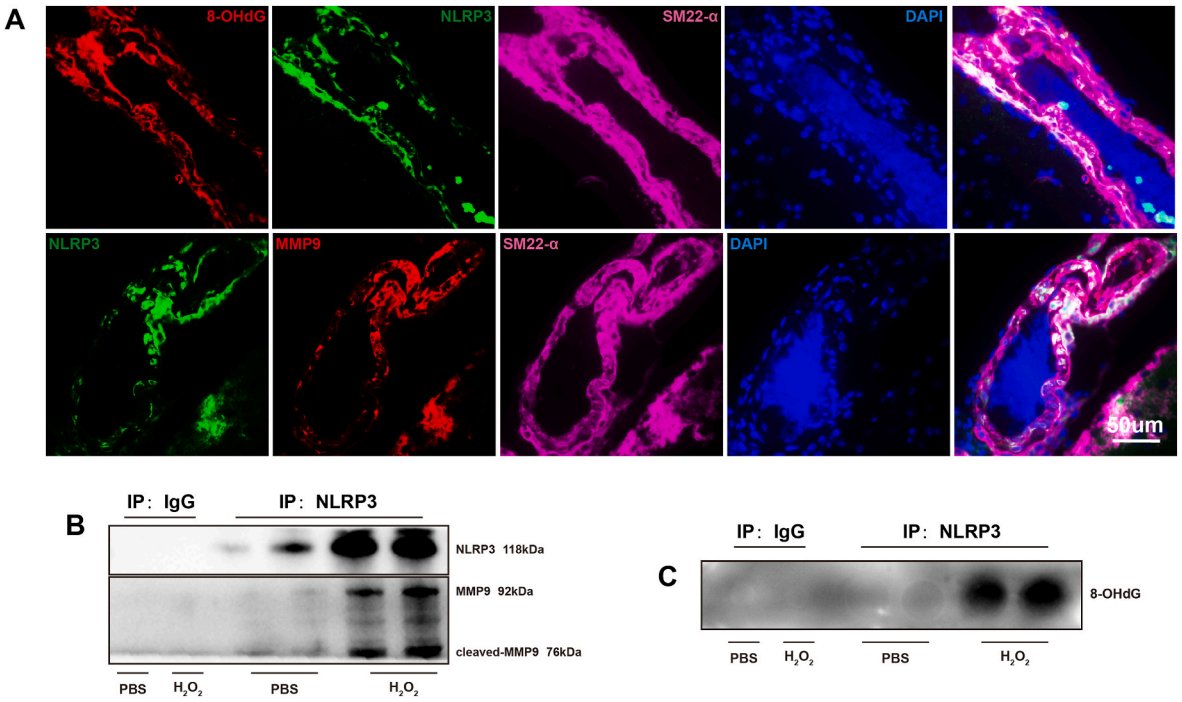

Fig. 7. NLRP3 binds to 8-OHdG and MMP9 in vascular smooth muscle cell of IA
A, Representative picture of multiple immunofluorescence staining shows that 8-OHdG (red), NLRP3 (green), and MMP9 (red) were co-localized in smooth muscle cells (purple) of IA wall at mice. B, Cell lysates were collected and immunoprecipitated with *anti*-NLRP3 Ab and *anti*-IgG Ab, then western blotted with *anti*-NLRP3 Ab and *anti*-MMP9 Ab. C, Cell lysates were collected and immunoprecipitated with *anti*-NLRP3 Ab and *anti*-IgG Ab, then dot blotted with anti-8-OHdG Ab.

that 8-OHdG has a direct combination with NLRP3, which further binds to MMP9 and promotes MMP9 activation.

3.6. Reduced the development of intracranial aneurysm and 8-OHdG/NLRP3/MMP9 pathway in wild-type (WT) mice treated with CsA

Having established the importance of cypD in IA development, we next investigated whether IA progression could be prevented or even reverted by pharmacologically inhibiting cypD activation in mice. Cyclosporin A (CsA), a clinically proven immunosuppressant, is currently the most-well studied cypD inhibitor. Interestingly, compared with the control group, mice treated with CsA significantly reduced the incidences of aneurysms (85% vs 46.67%, n = 17 vs n = 14, P = 0.008, Fig. 8A) and ruptured aneurysms (76.47% vs 35.71%, n = 13 vs n = 5, P = 0.0325, Fig. 8A). Similarly, a symptom-free curve also showed a significant reduction of aneurysmal rupture in IA mice treat with CsA (Fig. 8B). Moreover, there was no difference in blood pressure values between the two groups (Fig. 8C).

To characterize the effect of CsA treatment at the histological level, we observed less elastic fiber degradation and TUNEL positive VSMCs in the IA wall of mice treat with CsA than in those of mice without CsA treatment, which was similar with cypD KO mice (Fig. 8D–G). We next tested the therapeutic potential of CsA in 8-OHdG/NLRP3/MMP9 pathway, immunofluorescence staining in vivo revealed that CsA reduced the expression levels of 8-OHdG, NLRP3 and MMP9 (Fig. 9A–F). These data clearly indicate a protective effect of CsA against IA development.

4. Discussion

In this study, we identified a novel role of cypD in the pathogenesis of IA and the novel contributions included as following. First, we identified that cypD gene expression exhibited high fold change in both human and mouse from IA tissues, and cypD protein was upregulated in mice with IA. Moreover, global knockout of cypD protected mice against IA formation and rupture in previously explicit IA models. Furthermore, mechanistic studies in vivo and vitro identified that high expression of cypD binds to ATP5B to promote ROS release and activated 8-OHdG/NLRP3/MMP9 pathway, stimulated MMP9 production and cleaved, which accelerated VSMC apoptosis and elastic fiber degradation. Finally, we showed that pharmacologically inhibition of cypD with Cyclosporin A (CsA) mitigated IA development in mice by inhibiting 8-OHdG/NLRP3/MMP9 pathway. These findings suggest that cypD is a novel and critical molecule involved in IA progression.

It is well-established that cypD acts an extremely crucial role in the opening of mitochondrial permeability transition pore (mPTP) by interacting with ATP5B, which further facilities the output of ROS [13,23]. Damaged mitochondrion release a large amount of ROS that promotes VSMCs apoptosis and elastic fiber degradation, which have pivotal effect in IA development [6,8]. Several lines of evidence from experiments in pulmonary arterial, brain, platelets and liver have established that cypD facilitates the release of ROS for further oxidative stress, inflammation and cell death [14,18,24]. Astonishingly, cypD-absence was shown to reverse ROS production and improve vascular relaxation in the Angiotensin 2 induced aorta injury which is similar to the pathogenesis of IA [17]. But, it is still unknown whether cypD induced ROS output is answerable for IA development. In the present study, we found that the predominant higher expression of cypD mRNA and cypD protein in both human and mouse aneurysm lesions, especially in VSMCs. Additionally, potent evidence confirmed that cypD opens the mPTP to release ROS by directly binding to ATP5B, as evidenced by immunoprecipitation in our study. More importantly, global knockout of cypD resulted in a low levels of ROS and MMP9 in VSMCs, a low incidence of IA and rupture IA in DOCA-induced IA model, attenuated VSMCs apoptosis and decreased elastin degradation, highlighting the indispensable pernicious effects of cypD in IA. In addition to apoptosis, cypD has been shown to regulate necrosis in multiple disease including ischemic stroke and cardiac injury [24,25], future studies are necessary to determine whether cypD induced necrosis is important for IA progression.

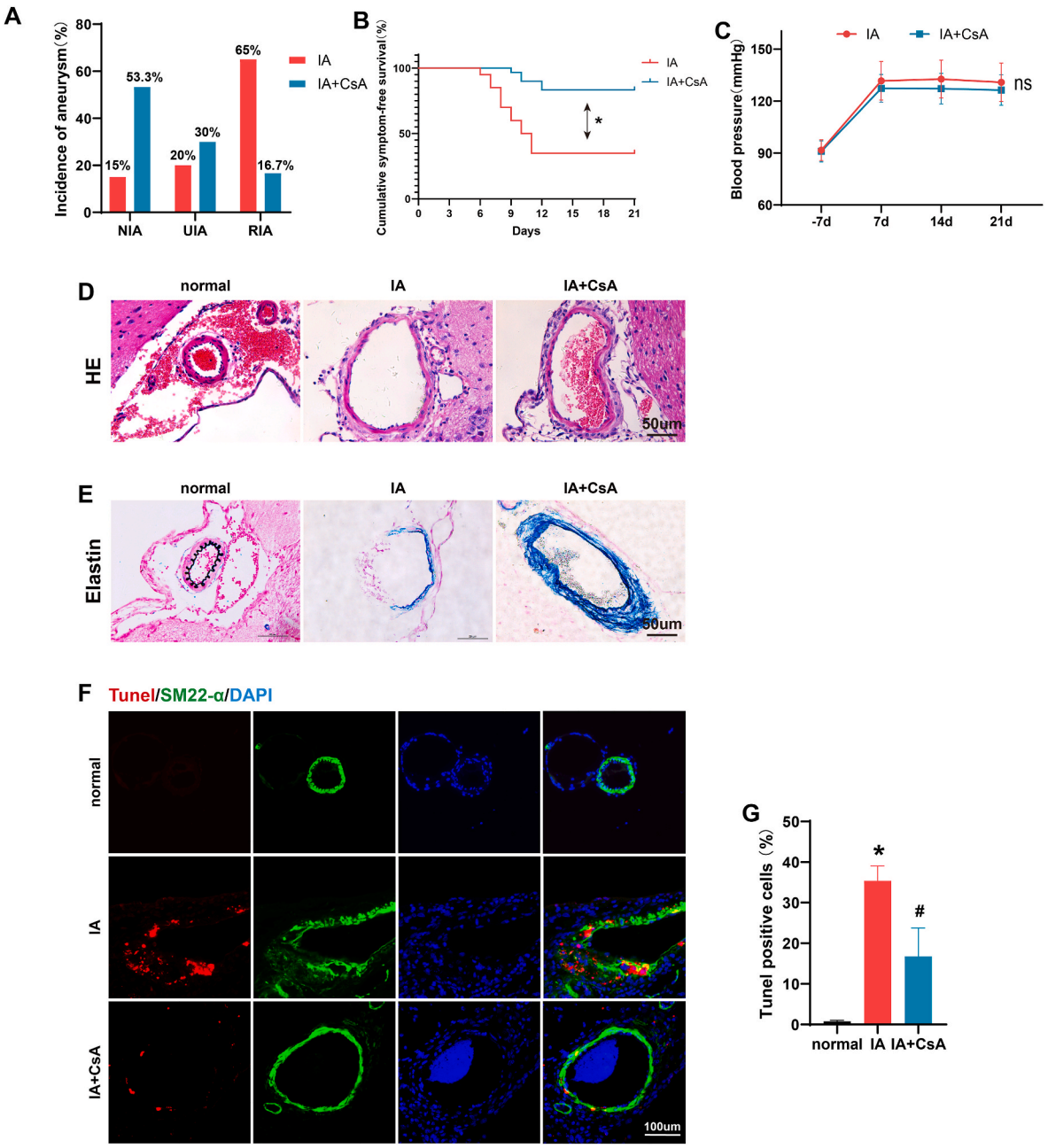

Fig. 8. CsA treatment reduced the development of intracranial aneurysm in wild-type (WT) mice
A, The incidence of IA and ruptured IA in IA group and IA mice treatment with CsA; B, The cumulative symptom-free survival in both groups. *P < 0.05. C, Blood pressure results in tow groups. D-E, Representative images of hematoxylin-eosin (HE) staining and elastic fiber satining in different groups. n = 4 per group. F-G, Representative microphotographs and quantitative analyses of TUNEL staining (red) co-localization on VSMCs (SM22-α, green) in different groups. n = 4 per group. Bars represent mean ± SD. ns stands for no significance; *P < 0.05 vs. Normal group; #P < 0.05 vs. IA group.

ROS is intimately involved in vascular remodeling and the pathophysiology of IA [26]. 8-OHdG, a product of DNA oxidation by ROS, is a master regulator of oxidative stress, inflammation and apoptosis and is considered to be an important marker of cardiovascular and cerebrovascular diseases [12,27,28]. Previous studies consistently showed that higher levels of 8-OHdG is correlated with poor prognosis in patients with coronary artery disease [29]. However, the distant contribution of 8-OHdG to IA pathogenesis has not been previously explored. Here, we show that 8-OHdG was upregulated in VSMCs of IA wall, and directly bind to NLRP3 in VSMCs leading to disease associated inflammatory responses. Interestingly, it is well established that oxidized DNA is essential for the activation of NLRP3 inflammasome in various disease models, contributing to inflammation and cell death [30–32]. More importantly, a positive correlation between NLRP3 expression level and aneurysm rupture in human IA patients was reported [33]. Therefore, 8-OHdG production correlating with the higher expression of NLRP3 is a significant evidence of 8-OHdG's role in accelerating IA progression. These findings reconfirmed that blocking ROS release could be a potential target for developing anti-inflammation interventions against IA development.

Moreover, oxidized DNA has recently been reported to exacerbate aortic degeneration by controlling SMC apoptosis via STING pathway, which is a widely reported inflammation signaling molecule in multiple diseases including vascular and immune [34,35]. These previous observations remind us that 8-OHdG may have several different downstream signaling, further studies are need to explore other downstream

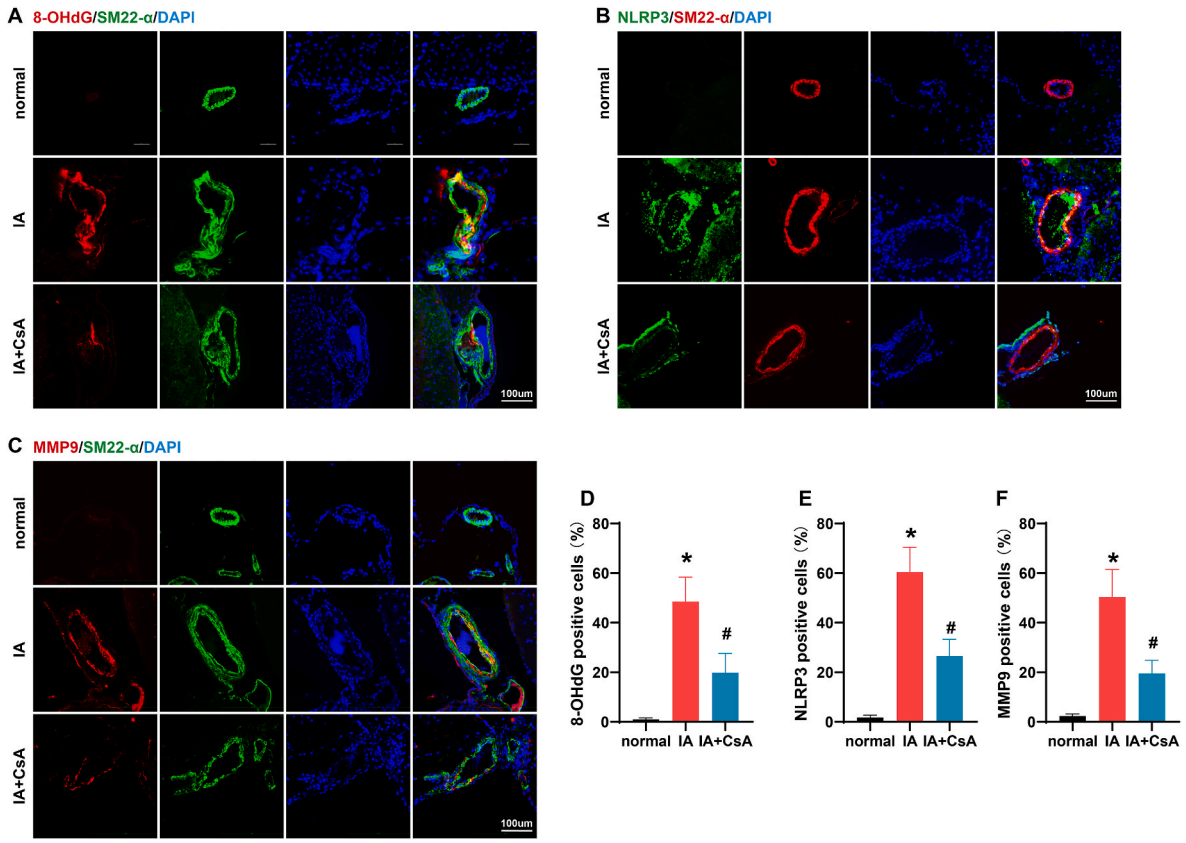

Fig. 9. CsA treatment down-regulates 8-OHdG/NLRP3/MMP9 pathway in wild-type (WT) mice with IA
A-F, Representative microphotographs of double immunofluorescence staining for 8-OHdG (red), NLRP3 (green) and MMP9 (red) in the VSMCs in diverse groups. n = 4 per group. Bars represent mean ± SD. ns stands for no significance; *P < 0.05 vs. Normal group; #P < 0.05 vs. IA group.

signals associated with 8-OHdG in VSMCs from IA patients.

Matrix metalloprotein 9 (MMP9), produced primarily by VSMCs and macrophages, are important mediators of the extracellular matrix degradation which are reported to be the shared pathological mechanisms in multiple vascular disease including IA, aortic aneurysm diseases (AADs) and atherosclerosis [36–39]. Macrophage-derived MMP9 acts an extremely vital role about extracellular matrix degradation in cardiovascular diseases, but does not appear to be important in IA. Because the clearance of macrophages could not reduce the production of MMPs in IA model [40]. Recent evidence suggested that VSMCs-derived MMP9 are responsible for IA lesion development [5]. Consistent with the previous findings, the present study showed that MMP9 upregulation from VSMCs dramatically promoted the degradation of elastic fibers and apoptosis. Inversely, MMP9 downregulation in VSMCs rescued elastic fibers, relieved apoptosis and prevented IA progression. Taken together, these findings demonstrated that MMP9, primarily from VSMCs, destroyed elastic fiber and accelerated VSMCs apoptosis to mediate IA progression.

Accumulating evidence implied the critical roles of MMP9 from VSMCs in IA progression, but the molecular mechanisms underlying MMP9 activation are poorly understood. Recently, NLRP3 inhibitor MCC950 was shown to restrain MMP9 expression and activation in multiple disease models, such as human umbilical vein endothelial cells and macrophages [41,42]. Accordingly, it is logical to conjecture that MMP9 activity may be alter by NLRP3. Intriguingly, our study exbihited that the expression changes of both NLRP3 and MMP9 are consistent, and NLRP3 directly bind and activate MMP9 in VSMCs, leading to the destruction of elastic fibers. These results indicated that NLRP3 is a crucial upstream of MMP9 and positively regulated MMP9 in VSMCs [43]. More importantly, the production of ROS exhibited enhanced expression and activity of MMP9 in osteoporosis, aortic dissection and cancer [44–46]. We further showed that the expression levels of 8-OHdG, NLRP3 and MMP9 were not only positively correlated, but also the interaction between them was confirmed by immunoprecipitation. So, it is reasonable to believe that the mechanism of MMP9 activation by ROS is via 8-OHdG/NLRP3 pathway in VSMCs of IA lesion, which was firstly mentioned in our paper. It is important to note that this finding can explain how ROS contributes to IA progression.

In conclusion, our studies demonstrated that cypD has a detrimental effect on VSMC apoptosis and elastic fiber degradation to expedite IA development. Mechanistically, cypD potently activated the 8-OHdG/NLRP3/MMP9 pathway by the accumulation of ROS. These findings identify that cypD inhibition as a potential target for hindering IA progression. Further studies are warranted to develop direct and specific cypD inhibitors to treat IA.

Authors' contributions

Conceptualization: H.F., C.D.; Methodology: H.F.; Investigation: H. F., H.T., F.J., S.S., Y.L, Z.W.; Writing: H.F.; Proofread: H.F., X.Z., X.H.; Funding: C.D., X.L., H.F.

Sources of funding

This study was supported by the National Natural Science Foundation Project (Grant number: 82271298, C.D.; Grant number: 82271297, X.L.) and President Foundation of Zhujiang Hospital, Southern Medical University (Grant number: 2023yzjj2022qn17, H.F.).

Declaration of competing interest

All the authors have approved the manuscript and agree with

submission to your esteemed journal. There are no conflicts of interest to declare.

Data availability

Data will be made available on request.

Appendix A. Supplementary data

Supplementary data to this article can be found online at https://doi.org/10.1016/j.redox.2023.102887.

References

[1] T. Krings, D.M. Mandell, T.-R. Kiehl, S. Geibprasert, M. Tymianski, H. Alvarez, et al., Intracranial aneurysms: from vessel wall pathology to therapeutic approach, Nat. Rev. Neurol. 7 (10) (2011) 547–559, https://doi.org/10.1038/nrneurol.2011.136.

[2] M.H. Li, S.W. Chen, Y.D. Li, Y.C. Chen, Y.S. Cheng, D.J. Hu, et al., Prevalence of unruptured cerebral aneurysms in Chinese adults aged 35 to 75 years: a cross-sectional study, Ann. Intern. Med. 159 (8) (2013) 514–521, https://doi.org/10.7326/0003-4819-159-8-201310150-00004.

[3] J. Claassen, S. Park, Spontaneous subarachnoid haemorrhage, Lancet 400 (10355) (2022) 846–862, https://doi.org/10.1016/s0140-6736(22)00938-2.

[4] M. Maher, T. Schweizer, R. Macdonald, Treatment of spontaneous subarachnoid hemorrhage: guidelines and gaps, Stroke 51 (4) (2020) 1326–1332, https://doi.org/10.1161/strokeaha.119.025997.

[5] R.M. Starke, N. Chalouhi, D. Ding, D.M. Raper, M.S. McKisic, G.K. Owens, et al., Vascular smooth muscle cells in cerebral aneurysm pathogenesis, Transl. Stroke Res. 5 (3) (2014) 338–346, https://doi.org/10.1007/s12975-013-0290-1.

[6] Z.H. Sun, F. Liu, L.L. Kong, P.M. Ji, L. Huang, H.M. Zhou, et al., Interruption of TRPC6-NFATC1 signaling inhibits NADPH oxidase 4 and VSMCs phenotypic switch in intracranial aneurysm, Biomed. Pharmacother. 161 (2023), 114480, https://doi.org/10.1016/j.biopha.2023.114480.

[7] Y. Zhang, P. Murugesan, K. Huang, H. Cai, NADPH oxidases and oxidase crosstalk in cardiovascular diseases: novel therapeutic targets, Nat. Rev. Cardiol. 17 (3) (2020) 170–194, https://doi.org/10.1038/s41569-019-0260-8.

[8] A.N. Martinez, G.G. Tortelote, C.L. Pascale, I.G. McCormack, K.D. Nordham, N. J. Suder, et al., Single-cell transcriptome analysis of the circle of willis in a mouse cerebral aneurysm model, Stroke 53 (8) (2022) 2647–2657, https://doi.org/10.1161/STROKEAHA.122.038776.

[9] M. Bonora, C. Giorgi, P. Pinton, Molecular mechanisms and consequences of mitochondrial permeability transition, Nat. Rev. Mol. Cell Biol. 23 (4) (2022) 266–285, https://doi.org/10.1038/s41580-021-00433-y.

[10] M. Pérez, D. Ponce, A. Aranguiz, M. Behrens, R. Quintanilla, Mitochondrial permeability transition pore contributes to mitochondrial dysfunction in fibroblasts of patients with sporadic Alzheimer's disease, Redox Biol. 19 (2018) 290–300, https://doi.org/10.1016/j.redox.2018.09.001.

[11] C. Gautier, E. Giaime, E. Caballero, L. Núñez, Z. Song, D. Chan, et al., Regulation of mitochondrial permeability transition pore by PINK1, Mol. Neurodegener. 7 (2012) 22, https://doi.org/10.1186/1750-1326-7-22.

[12] X-b Wang, N-h Cui, Xn Liu, X. Liu, Mitochondrial 8-hydroxy-2′-deoxyguanosine and coronary artery disease in patients with type 2 diabetes mellitus, Cardiovasc. Diabetol. 19 (1) (2020), https://doi.org/10.1186/s12933-020-00998-6.

[13] Q. Zhao, J. Liu, H. Deng, R. Ma, J.-Y. Liao, H. Liang, et al., Targeting mitochondria-located circRNA SCAR alleviates NASH via reducing mROS output, Cell 183 (1) (2020) 76–93.e22, https://doi.org/10.1016/j.cell.2020.08.009.

[14] H. Du, L. Guo, F. Fang, D. Chen, A.A. Sosunov, G.M. McKhann, et al., Cyclophilin D deficiency attenuates mitochondrial and neuronal perturbation and ameliorates learning and memory in Alzheimer's disease, Nat. Med. 14 (10) (2008) 1097–1105, https://doi.org/10.1038/nm.1868.

[15] N.V. Naoumov, Cyclophilin inhibition as potential therapy for liver diseases, J. Hepatol. 61 (5) (2014) 1166–1174, https://doi.org/10.1016/j.jhep.2014.07.008.

[16] X. Liu, H. Du, Q. Chai, Q. Jia, L. Liu, M. Zhao, et al., Blocking mitochondrial cyclophilin D ameliorates TSH-impaired defensive barrier of artery, Redox Biol. 15 (2018) 418–434, https://doi.org/10.1016/j.redox.2018.01.004.

[17] H.A. Itani, A.E. Dikalova, W.G. McMaster, R.R. Nazarewicz, A.T. Bikineyeva, D. G. Harrison, et al., Mitochondrial cyclophilin D in vascular oxidative stress and hypertension, Hypertension 67 (6) (2016) 1218–1227, https://doi.org/10.1161/HYPERTENSIONAHA.115.07085.

[18] M. Gierhardt, O. Pak, A. Sydykov, S. Kraut, J. Schaffer, C. Garcia, et al., Genetic deletion of p66shc and/or cyclophilin D results in decreased pulmonary vascular tone, Cardiovasc. Res. 118 (1) (2022) 305–315, https://doi.org/10.1093/cvr/cvaa310.

[19] T. Wu, E. Hu, S. Xu, M. Chen, P. Guo, Z. Dai, et al., clusterProfiler 4.0: a universal enrichment tool for interpreting omics data, Innovation 2 (3) (2021), 100141, https://doi.org/10.1016/j.xinn.2021.100141.

[20] K. Shimada, H. Furukawa, K. Wada, M. Korai, Y. Wei, Y. Tada, et al., Protective role of peroxisome proliferator-activated receptor-gamma in the development of intracranial aneurysm rupture, Stroke 46 (6) (2015) 1664–1672, https://doi.org/10.1161/STROKEAHA.114.007722.

[21] L. Huang, Y. Chen, R. Liu, B. Li, X. Fei, X. Li, et al., P-glycoprotein aggravates blood brain barrier dysfunction in experimental ischemic stroke by inhibiting endothelial autophagy, Aging Dis. 13 (5) (2022) 1546–1561, https://doi.org/10.14336/AD.2022.0225.

[22] H. Fan, R. Ding, W. Liu, X. Zhang, R. Li, B. Wei, et al., Heat shock protein 22 modulates NRF1/TFAM-dependent mitochondrial biogenesis and DRP1-sparked mitochondrial apoptosis through AMPK-PGC1alpha signaling pathway to alleviate the early brain injury of subarachnoid hemorrhage in rats, Redox Biol. 40 (2021), 101856, https://doi.org/10.1016/j.redox.2021.101856.

[23] J. Karch, M. Bround, H. Khalil, M. Sargent, N. Latchman, N. Terada, et al., Inhibition of mitochondrial permeability transition by deletion of the ANT family and CypD, Sci. Adv. 5 (8) (2019), eaaw4597, https://doi.org/10.1126/sciadv.aaw4597.

[24] F. Denorme, B.K. Manne, I. Portier, A.S. Eustes, Y. Kosaka, B.T. Kile, et al., Platelet necrosis mediates ischemic stroke outcome in mice, Blood 135 (6) (2020) 429–440, https://doi.org/10.1182/blood.2019002124.

[25] K. Wang, T. An, L.Y. Zhou, C.Y. Liu, X.J. Zhang, C. Feng, et al., E2F1-regulated miR-30b suppresses Cyclophilin D and protects heart from ischemia/reperfusion injury and necrotic cell death, Cell Death Differ. 22 (5) (2015) 743–754, https://doi.org/10.1038/cdd.2014.165.

[26] R.M. Starke, J.W. Thompson, M.S. Ali, C.L. Pascale, A. Martinez Lege, D. Ding, et al., Cigarette smoke initiates oxidative stress-induced cellular phenotypic modulation leading to cerebral aneurysm pathogenesis, Arterioscler. Thromb. Vasc. Biol. 38 (3) (2018) 610–621, https://doi.org/10.1161/ATVBAHA.117.310478.

[27] K. Sun, J. Fan, J. Han, Ameliorating effects of traditional Chinese medicine preparation, Chinese materia medica and active compounds on ischemia/reperfusion-induced cerebral microcirculatory disturbances and neuron damage, Acta Pharm. Sin. B 5 (1) (2015) 8–24, https://doi.org/10.1016/j.apsb.2014.11.002.

[28] S. Kobayashi, T. Susa, T. Tanaka, Y. Wada, S. Okuda, M. Doi, et al., Urinary 8-hydroxy-2'-deoxyguanosine reflects symptomatic status and severity of systolic dysfunction in patients with chronic heart failure, Eur. J. Heart Fail. 13 (1) (2011) 29–36, https://doi.org/10.1093/eurjhf/hfq178.

[29] A. Di Minno, L. Turnu, B. Porro, I. Squellerio, V. Cavalca, E. Tremoli, et al., 8-Hydroxy-2-Deoxyguanosine levels and cardiovascular disease: a systematic review and meta-analysis of the literature, Antioxidants Redox Signal. 24 (10) (2016) 548–555, https://doi.org/10.1089/ars.2015.6508.

[30] S. Li, H. Li, Y.L. Zhang, Q.L. Xin, Z.Q. Guan, X. Chen, et al., SFTSV infection induces BAK/BAX-Dependent mitochondrial DNA release to trigger NLRP3 inflammasome activation, Cell Rep. 30 (13) (2020) 4370–43785 e7, https://doi.org/10.1016/j.celrep.2020.02.105.

[31] Z. Zhong, S. Liang, E. Sanchez-Lopez, F. He, S. Shalapour, X.J. Lin, et al., New mitochondrial DNA synthesis enables NLRP3 inflammasome activation, Nature 560 (7717) (2018) 198–203, https://doi.org/10.1038/s41586-018-0372-z.

[32] L.K. Billingham, J.S. Stoolman, K. Vasan, A.E. Rodriguez, T.A. Poor, M. Szibor, et al., Mitochondrial electron transport chain is necessary for NLRP3 inflammasome activation, Nat. Immunol. 23 (5) (2022) 692–704, https://doi.org/10.1038/s41590-022-01185-3.

[33] D. Zhang, H. Yan, Y. Hu, Z. Zhuang, Z. Yu, C. Hang, Increased expression of NLRP3 inflammasome in wall of ruptured and unruptured human cerebral aneurysms: preliminary results, J. Stroke Cerebrovasc. Dis. 24 (5) (2015) 972–979, https://doi.org/10.1016/j.jstrokecerebrovasdis.2014.12.019.

[34] W. Luo, Y. Wang, L. Zhang, P. Ren, C. Zhang, Y. Li, et al., Critical role of cytosolic DNA and its sensing adaptor STING in aortic degeneration, dissection, and rupture, Circulation 141 (1) (2020) 42–66, https://doi.org/10.1161/CIRCULATIONAHA.119.041460.

[35] V. Kumar, C. Bauer, JHt Stewart, Targeting cGAS/STING signaling-mediated myeloid immune cell dysfunction in TIME, J. Biomed. Sci. 30 (1) (2023) 48, https://doi.org/10.1186/s12929-023-00942-2.

[36] D. Cai, C. Sun, G. Zhang, X. Que, K. Fujise, N.L. Weintraub, et al., A novel mechanism underlying inflammatory smooth muscle phenotype in abdominal aortic aneurysm, Circ. Res. 129 (10) (2021) e202–e214, https://doi.org/10.1161/CIRCRESAHA.121.319374.

[37] Y. Ishida, Y. Kuninaka, M. Nosaka, A. Kimura, A. Taruya, M. Furuta, et al., Prevention of CaCl(2)-induced aortic inflammation and subsequent aneurysm formation by the CCL3-CCR5 axis, Nat. Commun. 11 (1) (2020) 5994, https://doi.org/10.1038/s41467-020-19763-0.

[38] S. Ju, L. Lim, Y.J. Ki, D.H. Choi, H. Song, Oxidative stress generated by polycyclic aromatic hydrocarbons from ambient particulate matter enhance vascular smooth muscle cell migration through MMP upregulation and actin reorganization, Part. Fibre Toxicol. 19 (1) (2022) 29, https://doi.org/10.1186/s12989-022-00472-z.

[39] D.M. Sawyer, L.A. Pace, C.L. Pascale, A.C. Kutchin, B.E. O'Neill, R.M. Starke, et al., Lymphocytes influence intracranial aneurysm formation and rupture: role of extracellular matrix remodeling and phenotypic modulation of vascular smooth muscle cells, J. Neuroinflammation 13 (1) (2016) 185, https://doi.org/10.1186/s12974-016-0654-z.

[40] M. Mandelbaum, J. Kolega, J.M. Dolan, A.H. Siddiqui, H. Meng, A critical role for proinflammatory behavior of smooth muscle cells in hemodynamic initiation of intracranial aneurysm, PLoS One 8 (9) (2013), e74357, https://doi.org/10.1371/journal.pone.0074357.

[41] P. Ren, D. Wu, R. Appel, L. Zhang, C. Zhang, W. Luo, et al., Targeting the NLRP3 inflammasome with inhibitor MCC950 prevents aortic aneurysms and dissections in mice, J. Am. Heart Assoc. 9 (7) (2020), e014044, https://doi.org/10.1161/JAHA.119.014044.

[42] Y. Dai, J. Zhang, J. Xiang, Y. Li, D. Wu, J. Xu, Calcitriol inhibits ROS-NLRP3-IL-1beta signaling axis via activation of Nrf2-antioxidant signaling in hyperosmotic stress stimulated human corneal epithelial cells, Redox Biol. 21 (2019), 101093, https://doi.org/10.1016/j.redox.2018.101093.

[43] T. Yamaguchi, T. Miyamoto, E. Shikata, I. Yamaguchi, K. Shimada, K. Yagi, et al., Activation of the NLRP3/IL-1beta/MMP-9 pathway and intracranial aneurysm rupture associated with the depletion of ERalpha and Sirt1 in oophorectomized rats, J. Neurosurg. 138 (1) (2023) 191–198, https://doi.org/10.3171/2022.4.JNS212945.

[44] W. Liu, W. Zhang, T. Wang, J. Wu, X. Zhong, K. Gao, et al., Obstructive sleep apnea syndrome promotes the progression of aortic dissection via a ROS- HIF-1alpha-MMPs associated pathway, Int. J. Biol. Sci. 15 (13) (2019) 2774–2782, https://doi.org/10.7150/ijbs.34888.

[45] K. Chen, P. Qiu, Y. Yuan, L. Zheng, J. He, C. Wang, et al., Pseurotin A inhibits osteoclastogenesis and prevents ovariectomized-induced bone loss by suppressing reactive oxygen species, Theranostics 9 (6) (2019) 1634–1650, https://doi.org/10.7150/thno.30206.

[46] L. Walter, B. Canup, A. Pujada, T.A. Bui, B. Arbasi, H. Laroui, et al., Matrix metalloproteinase 9 (MMP9) limits reactive oxygen species (ROS) accumulation and DNA damage in colitis-associated cancer, Cell Death Dis. 11 (9) (2020) 767, https://doi.org/10.1038/s41419-020-02959-z.